Int. J. Heat Mass Transfer. Vol. 34, No. 8, pp. 2149–2163, 1991
Printed in Great Britain

0017-9310/91 $3.00+0.00
Pergamon Press plc

Natural convection arising from a heat generating substrate-mounted protrusion in a liquid-filled two-dimensional enclosure

SANJEEV B. SATHE
IBM Corporation, Endicott, NY 13760, U.S.A.

and

YOGENDRA JOSHI
Department of Mechanical Engineering, Naval Postgraduate School, Monterey, CA 93943, U.S.A.

(*Received* 10 *April* 1990 *and in final form* 16 *October* 1990)

Abstract—An investigation of natural convection flow and heat transfer arising from a substrate-mounted protruding heat source immersed in a liquid-filled square enclosure is reported. The model considers heat transfer within the protrusion and substrate and the coupled natural convection in the fluid. Numerical predictions are obtained for a wide range of appropriate Rayleigh and Prandtl numbers and substrate to fluid thermal conductivity ratios that may be encountered in liquid-immersion cooling of electronic components. For many situations of interest prescribing simplistic heat transfer conditions at the solid surfaces is found inappropriate. Increasing the Rayleigh number beyond 10^6 and the substrate thermal conductivity beyond 100 times that of the liquid produces only a marginal decrease in the maximum temperatures. Computed protrusion surface temperatures compare favorably with available experimental results for a similar configuration.

1. INTRODUCTION

THE STEADY increase in the volumetric heat generation rates within modern electronic chips due to the large and very large scale integration technologies is well known. If this current trend continues, the future development of reliable electronic components could well be restricted by the inability to maintain the device junction temperatures below the maximum specified limits. Thus the need for efficient cooling has assumed an ever important role. Chu [1] and Nakayama [2] described the various cooling techniques currently being examined to meet the reliability requirements of modern electronic packages.

A number of studies utilizing convective cooling are discussed by Incropera [3]. Passive cooling using natural convection is characterized by advantages such as simplicity of design, absence of noise and high reliability. Moreover, in the event of a failure of other cooling techniques, natural convection may be the only available mode. It is not surprising then that a few studies on natural convection from discrete heat sources to extensive ambient air have appeared recently [4–6].

Jaluria [4] considered discrete heat sources flush-mounted on a vertical adiabatic surface. The heaters were idealized as uniform heat flux regions. Lee and Yovanovich [5] idealized the flush heaters as uniform flux regions and accounted for one-dimensional conduction in the thin substrate. They also included surface radiation. Afrid and Zebib [6] studied protruding heat sources mounted on an adiabatic vertical surface. Both the natural convection in the air and conduction within the protrusion were included. For a single source, it was found that the maximum temperature varied linearly with the heat generation rate. The finite thermal conductivity of the substrate is likely to moderate this rate of increase in actual applications.

Natural convection in liquids has the added advantage of higher cooling rates compared to those in air for a given temperature difference. The use of liquid necessitates the presence of an enclosure. In many applications involving the packaging of high dissipation equipment such as power supplies, hermetically sealed units may be employed. A number of experimental studies have been performed on natural convection from discrete heat sources inside liquid-filled enclosures [7–13]. A few computational studies have also appeared. Lee *et al.* [14] studied two-dimensional natural convection in enclosures with discrete heat sources mounted on an adiabatic vertical wall. The heat sources were maintained at a predetermined arbitrary constant temperature. They confirmed the two cell flow structure observed experimentally in ref. [10]. Liu *et al.* [15] conducted a three-dimensional study to simulate the behavior of chips inside a liquid-filled enclosure. The protruding chip surfaces were simulated as constant heat flux regions on an adiabatic vertical wall.

In most applications the thermal conditions on the electronic package surfaces are unknown. For given input power level, the temperature distribution within the heat source, including the magnitude and location of the maximum temperature are of interest. None of the previous studies appear to have addressed the coupled heat transfer processes occurring within the heat source, the substrate and the liquid in a liquid-filled enclosure.

The aim of this work is to examine the steady-state conjugate heat transfer and natural convection arising

NOMENCLATURE

c_p specific heat at constant pressure [J kg^{-1} K^{-1}]
d dimension in Fig. 1 [m]
d_t substrate thickness [m]
g gravitational acceleration [m s^{-2}]
h protrusion height [m]
H enclosure height [m]
I function in equation (7)
k thermal conductivity [W m^{-1} K^{-1}]
L_t dimension in Fig. 1 [m]
n unit vector in the outward normal direction to the solid surface
p pressure [N m^{-2}]
P non-dimensional pressure, $p/\rho U_0^2$
Pr Prandtl number, $\mu c_p/k_f$
Q heat generation rate per unit length [W m^{-1}]
Q non-dimensional heat flux crossing the solid surface, equation (8)
R_c protrusion to fluid thermal conductivity ratio, k_c/k_f
R_s substrate to fluid thermal conductivity ratio, k_s/k_f
Ra Rayleigh number, $g\beta Qh^3/\alpha k_f \nu$
s non-dimensional clockwise contour distance along the solid–fluid interface in Table 1
S_b, S_t dimensions in Fig. 1 [m]
t_c enclosure wall temperature [K]
T non-dimensional temperature, $(t-t_c)/(Q/k_f)$
u vertical velocity component [m s^{-1}]
U non-dimensional vertical velocity component, u/U_0
U_0 reference velocity, $(g\beta Qh/k_f)^{1/2}$ [m s^{-1}]
v horizontal velocity component [m s^{-1}]
V non-dimensional horizontal velocity component, v/U_0
w protrusion width [m]
x vertical coordinate [m]
x_p distance above the center of the heat source [m]
X non-dimensional vertical coordinate, x/h
X_p non-dimensional vertical distance, x_p/h
y horizontal coordinate [m]
Y non-dimensional horizontal coordinate, y/h.

Greek symbols
α fluid thermal diffusivity [m^2 s^{-1}]
β coefficient of thermal expansion [K^{-1}]
μ dynamic viscosity [kg m^{-1} s^{-1}]
ν kinematic viscosity [m^2 s^{-1}]
ρ fluid density [kg m^{-3}].

Subscripts
c protrusion (chip)
f fluid/liquid
max maximum
s substrate.

from a substrate-mounted heated protrusion immersed in a two-dimensional fluid-filled enclosure. The enclosure boundaries are maintained at a constant temperature. Uniform volumetric heat generation takes place inside the protrusion. Neither the thermal conditions at the protrusion surfaces nor its temperature distribution are assumed to be known a priori. The appropriate governing equations are solved using a control-volume based finite-difference technique. For the limiting case of a vanishingly small protrusion mounted on an adiabatic substrate, computed surface temperatures above the heat source are compared with the wall-plume similarity solution. The effects of the fluid properties, heat generation level and the substrate conductivity on the heat transfer and fluid flow in the enclosure are next examined via a parametric study. Finally a comparison of the protrusion surface temperatures with available experimental data is presented.

2. MATHEMATICAL FORMULATION

The schematic diagram of the configuration examined is shown in Fig. 1. A protruding heat source mounted on a vertical substrate is immersed in a two-dimensional fluid-filled enclosure of height H and aspect ratio 1. The shaded region represents the protrusion and the substrate. Uniform volumetric heat generation takes place in the protrusion. The enclosure boundaries are maintained at a constant temperature, t_c. The protrusion, the substrate and the fluid have constant but different thermophysical properties. Assuming a steady-state, laminar flow with no viscous dissipation and the Boussinesq approximation to be true, the dimensionless governing equations can be written as follows:

fluid region

$$\frac{\partial U}{\partial X}+\frac{\partial V}{\partial Y}=0 \tag{1}$$

$$\frac{\partial (U^2)}{\partial X}+\frac{\partial (UV)}{\partial Y}=(Pr/Ra)^{1/2}\left(\frac{\partial^2 U}{\partial X^2}+\frac{\partial^2 U}{\partial Y^2}\right)+T-\frac{\partial P}{\partial X} \tag{2}$$

$$\frac{\partial (UV)}{\partial X}+\frac{\partial (V^2)}{\partial Y}=(Pr/Ra)^{1/2}\left(\frac{\partial^2 V}{\partial X^2}+\frac{\partial^2 V}{\partial Y^2}\right)-\frac{\partial P}{\partial Y} \tag{3}$$

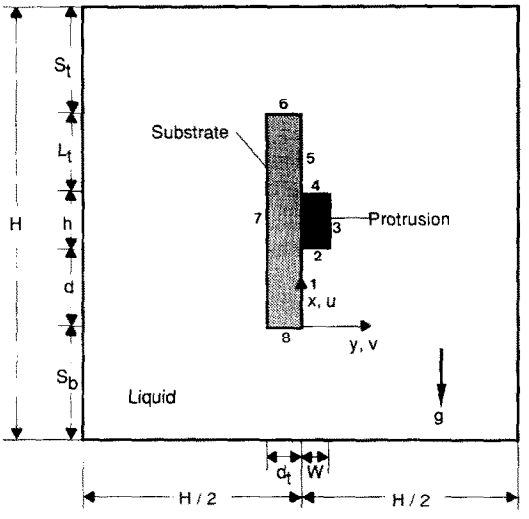

FIG. 1. Schematic diagram of the enclosure with a substrate-mounted protruding heat source.

$$\frac{\partial(UT)}{\partial X}+\frac{\partial(VT)}{\partial Y}=(1/Ra\,Pr)^{1/2}\left(\frac{\partial^2 T}{\partial X^2}+\frac{\partial^2 T}{\partial Y^2}\right); \quad (4)$$

solid region (protrusion)

$$\frac{\partial^2 T}{\partial X^2}+\frac{\partial^2 T}{\partial Y^2}=\frac{h}{wR_c}; \quad (5)$$

solid region (substrate)

$$\frac{\partial^2 T}{\partial X^2}+\frac{\partial^2 T}{\partial Y^2}=0; \quad (6)$$

where $X=x/h$, $Y=y/h$, $U=u/U_0$, $V=v/U_0$, $T=(t-t_c)/(Q/k_f)$, $P=p/\rho U_0^2$; $U_0=(g\beta Qh/k_f)^{1/2}$, $Pr=\mu c_p/k_f$, $Ra=g\beta Qh^3/\alpha k_f\nu$, $R_c=k_c/k_f$ and $R_s=k_s/k_f$. The various symbols are given in the Nomenclature.

The boundary conditions constitute isothermal enclosure walls at temperature t_c and the no-slip and impermeable wall conditions for the velocity components; i.e. $U=V=T=0$ at the enclosure walls. Heat fluxes are appropriately matched at the interfaces of dissimilar materials. The following parameters emerge as a result of the non-dimensionalization of the governing equations, boundary and matching conditions: Ra, Pr, R_c, R_s, S_b/h, d/h, L_t/h, S_t/h, d_t/h and w/h. The definitions of the symbols can be found in the Nomenclature.

3. METHOD OF SOLUTION

The governing equations are discretized using a finite-difference scheme wherein the control volumes for the temperature and pressure are staggered from those for the velocities. Power law profiles are used for the spatial variation of the dependent variables to ensure realistic results for a wide range of the grid Peclet numbers. Interface diffusivities are calculated using a harmonic-mean formulation in order to handle abrupt changes in the material properties. The details of the discretization process can be found in Patankar [16].

The discretized equations were solved iteratively using the line-by-line TDMA (Tri-Diagonal Matrix Algorithm) and the SIMPLER procedure as outlined in ref. [16]. It is noted that even though separate equations are written for the fluid and solid regions, the solid region is numerically simulated by letting its viscosity be very large. Thus the same momentum equation is solved throughout the computational domain. Similarly, for the energy equation, heat sources and property values are appropriately specified in each region and only one energy equation is solved. The flux matching conditions are used implicitly in the control volume formulation wherein mass, momentum and energy balances are incorporated for individual control volumes [16].

Test computations were performed on a series of grids ranging from 10×10 to 60×60 control volumes to determine the grid size effect. The values and locations for the maximum temperature and peak velocities did not change appreciably when the grid was refined beyond 40×40 control volumes. Unless mentioned otherwise, all the calculations reported hereafter are on a non-uniform mesh of 45×50 control volumes and represent a reasonable compromise between computational cost and accuracy. The grid points were densely packed above the protrusion after preliminary runs on coarser grids showed that the flow was thermally stratified below the protrusion. The iterations were terminated when the change in the dependent variables in successive iterations was no more than 0.005%. In most cases, an overall energy balance of less than 0.1% was achieved, with the energy balance in the worst case being no more than 1%. The overall energy balance was computed as the difference between the rates of total heat generation and total energy loss through the four walls of the enclosure.

The computational times on an IBM-370/3033 computer ranged widely from 200 to 600 CPU min for calculations started with $U=V=T=0$ throughout the cavity as the initial guess. The run times could be reduced in a few cases when computations were commenced with previously computed solutions as initial guesses.

4. COMPARISON WITH SIMILARITY SOLUTION

The present numerical procedure was validated by comparing the substrate surface temperatures above the protrusion (temperatures on face 5 in Fig. 1) with the predictions of a similarity solution for appropriate limiting conditions. The similarity solution considered is that of a wall plume arising from a line source placed at the leading edge of a vertical adiabatic wall. The

non-dimensional surface temperature rise above the source, T, is [17]

$$T = (64Ra\,Pr^3 I^4)^{-0.2} X_p^{-0.6} \quad (7)$$

where X_p is the non-dimensional vertical distance from the heated line source in the upward direction and I a numerically computed function of Pr [17].

The line source was simulated in the present computations by choosing the length of the substrate much larger than the protrusion height. An R_s value of 10^{-10} was chosen to simulate an adiabatic substrate wall. The enclosure boundaries were moved far away from the heat source by selecting $L_t/h = 20$ and $S_t/h = 5$. The numerical calculations were performed using a 60×60 mesh. It was found that the computational time was ten times larger than the other runs in this study, and thus a comparison for only one set of parameters is reported. The numerical prediction is for $Ra = 10^5$, $Pr = 5$, $R_c = 100$, $R_s = 10^{-10}$, $S_b/h = 2$, $d/h = 0.1$, $d_t/h = 0.15$ and $w/h = 0.15$.

Seen in Fig. 2 is a comparison of the non-dimensional temperatures obtained from the numerical simulation and those predicted by equation (7). The distance X_p is the distance from the mid-height of the protrusion (i.e. $X = 0.5$) for the numerical solutions. Since the heat source has a finite height, it is expected that the wall plume solution and the numerical computations will not agree very well for small X_p. The figure shows that when X_p is increased beyond 6, the agreement gets better. Such a trend was also observed in the investigation of Jaluria [4], wherein a discrete heat source was considered on a vertical adiabatic wall, and the boundary layer equations were solved numerically. The discrepancy between the analytical and the numerical solution is less than 10% for $6 < X_p < 11$. As X_p increases beyond 10, the discrepancy becomes worse. Such a trend is somewhat expected due to the fact that far enough from the protrusion and closer to the top wall, the wall plume type of flow is modified due to the presence of the top wall. Also, the discrepancy is in the right direction. Due to the recirculation of the flow caused by the presence of the top wall, hotter fluid gets entrained into the main plume flow, compared to the situation when the top wall is absent. Thus, the numerically predicted substrate surface temperatures are higher than those predicted from the wall plume solution for $X_p > 11$.

5. PARAMETRIC STUDY

Numerical computations were performed for a wide range of Ra, Pr and R_s that may be encountered in actual applications. The highest value of Ra in this investigation was primarily limited by the non-convergence of the numerical scheme. Calculations were performed for $Ra \leqslant 10^7$. To get an idea of the actual heating rates, for example, a power input of 0.1 W in a 10 mm × 10 mm × 25 mm long protruding source in commercially available dielectric fluids fluorinerts FC-75 and FC-71 [18] resulted in Ra of the order of 10^7 and 10^5, respectively. In water and air the corresponding values were 10^5 and 10^4, respectively.

The fluorinert dielectric liquids commonly used in

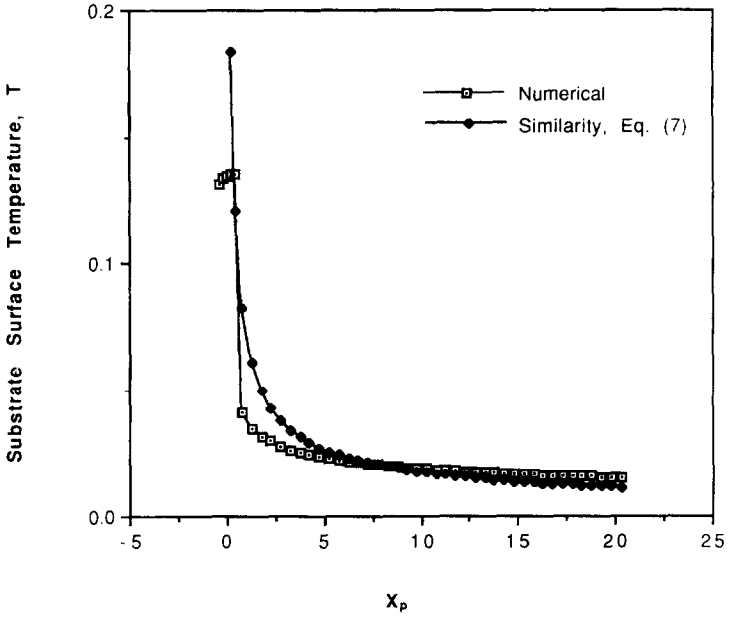

FIG. 2. Comparison of the numerically predicted substrate–fluid interface temperatures with the wall plume solution, equation (7). The distance X_p for the numerical predictions is measured from the mid-height of the protrusion.

liquid-immersion cooling are characterized by Pr much larger than 1. A few computations for $Pr = 10$, 10^2 and 10^3 revealed that increasing Pr from 10 to 10^3, other parameters remaining identical, produced a negligible change in the dimensionless temperatures within the solid. All results that follow are therefore for $Pr = 10$. In practical situations, the thermal conductivity of the substrate, k_s, may vary over a wide range from 0.1 W m^{-1} K^{-1} for epoxy-glass to 100 W m^{-1} K^{-1} for silicon carbide. The thermal conductivities of the fluorinert liquids are of the order of 0.1 W m^{-1} K^{-1} [18]. Thus the ratio $R_s = k_s/k_f$ ranges from 1 to 10^3. Computations were extended to $R_s = 0.1$ for the sake of completeness.

The geometric parameters used in all calculations are as follows: $S_b/h = 2.5$, $d/h = 2$, $L_t/h = 2$, $S_t/h = 2.5$, $d_t/h = 1.5$ and $w/h = 0.75$. The protrusion to fluid thermal conductivity ratio, R_c, is kept constant at 100 for all the calculations.

5.1. *Effect of Ra*

The streamlines and isotherms are shown in Fig. 3 for $Ra = 10^3$, 10^4, 10^5 and 10^6, all for $R_s = 1$. For Ra ranging from approximately 10^2 (not shown) to 10^4 the flow patterns were quite similar. The flow rising from the heated protrusion travels almost vertically upwards and splits to form two cells on the left- and right-hand sides of the substrate. The eddy centers shift upwards as Ra increases. The left side eddy is a secondary eddy formed as a net result of the splitting of the flow at the top and the weak heating via conduction through the substrate. The fluid in the right-hand bottom corner remains virtually stagnant. At $Ra \approx 10^5$ a considerable change occurs in the flow pattern behind the substrate. The secondary eddy moves directly above the substrate, instead of at the back of the substrate.

An increase in Ra diminishes the importance of substrate conduction, as evident from the relative strengths of the primary and secondary cells. It also brings about a slight bending of the main flow towards the right above the protrusion as it leaves the substrate wall. The bending is clearly evident for $Ra = 10^6$. Also, for $Ra > 10^5$, weak shear driven eddies appear in the bottom half of the enclosure. The isotherms indicate a thermally stratified region in the lower half

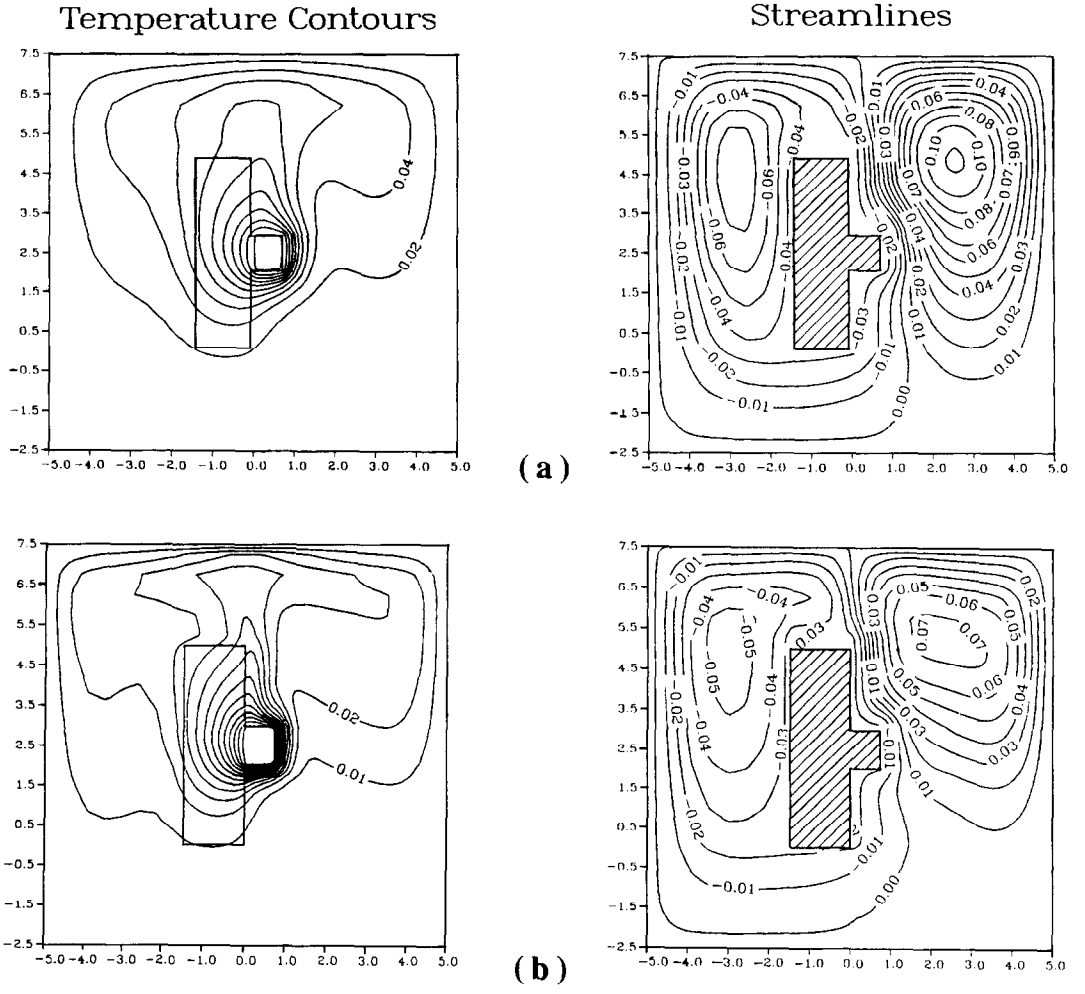

FIG. 3. Streamline and temperature contours for (a) $Ra = 10^3$, (b) $Ra = 10^4$, (c) $Ra = 10^5$ and (d) $Ra = 10^6$. The computations are for $Pr = 10$, $R_s = 1$ and $R_c = 100$.

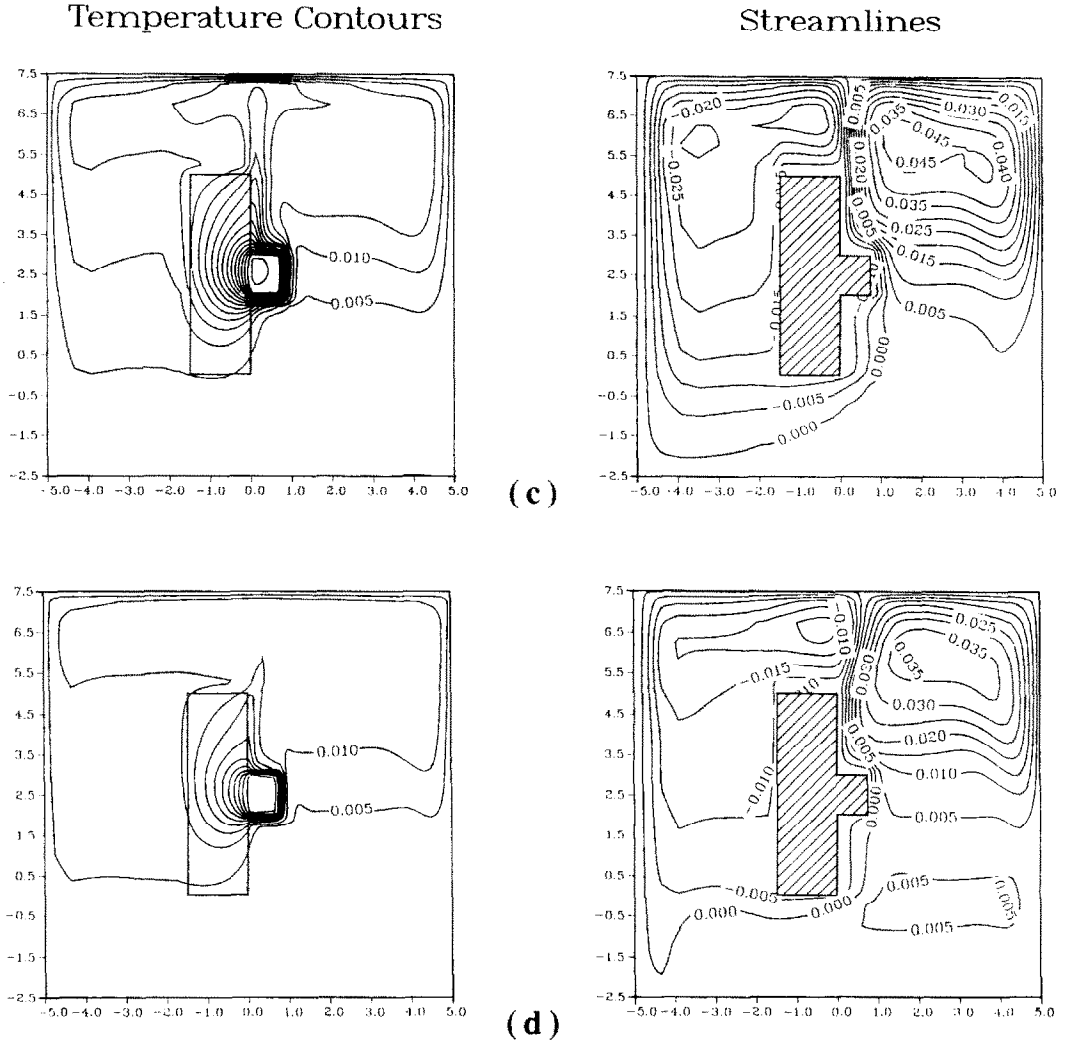

FIG. 3. — *Continued.*

of the enclosure, with the level of stratification increasing at higher *Ra*. The thermal gradients near the top wall become steeper as *Ra* increases.

Plotted in Fig. 4 are the dimensionless solid surface temperatures for different *Ra*. These are calculated by using a harmonic mean formulation since the control-volume nodes for the temperatures do not lie on the interfaces that separate two different materials. The quantity s is the clockwise contour distance along the solid surface starting from the origin. Table 1 gives the ranges of s corresponding to the different surfaces numbered in Fig. 1. The temperatures are highest at the protrusion–fluid interface. The protrusion faces are almost isothermal due to the high protrusion thermal conductivity. From the definition of *Ra* it is clear that for the same heating rate, a higher *Ra* implies a greater buoyant force. It is thus expected that an increase in *Ra* would enhance cooling of the heat source. Indeed Fig. 4 reveals an almost four-fold drop in the dimensionless protrusion face temperatures when *Ra* is increased from 10^3 to 10^6. This drop is not linear with a change in *Ra* but is lower when *Ra* is higher.

The present results thus clearly indicate that the temperatures within the solid must be obtained

Table 1. Ranges of s corresponding to different solid–fluid interfaces

Surface No. in Fig. 1	X	Y	s
1	0 to 2	0	0.00 to 2.00
2	2	0.0 to 0.75	2.00 to 2.75
3	2 to 3	0.75	2.75 to 3.75
4	3	0.0 to 0.75	3.75 to 4.50
5	3 to 5	0	4.50 to 6.50
6	5	−1.5 to 0	6.50 to 8.00
7	0 to 5	−1.5	8.00 to 13.00
8	0	−1.5 to 0	13.00 to 14.50

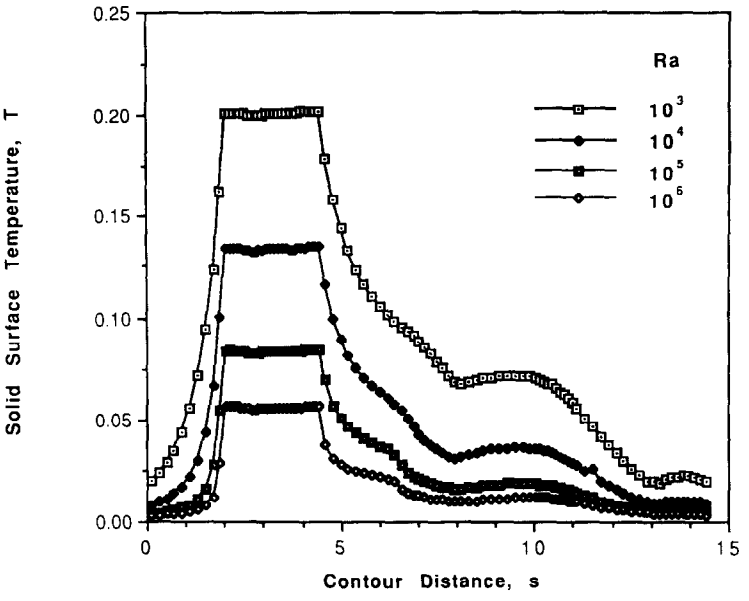

FIG. 4. Solid–fluid interface temperatures for different Ra. The distance s is the contour length along the interface as defined in Table 1. The computations are for $Pr = 10$, $R_s = 1$ and $R_c = 100$.

through a conjugate heat transfer analysis. The temperatures of the substrate surface below the protrusion ($s < 2$) show an increasing thermal stratification in the portion below the protrusion as Ra increases. For example, as s is increased from 0 to 2, the temperatures for $Ra = 10^3$ increase comparatively gradually, whereas for $Ra = 10^6$, the temperatures increase abruptly very near the protrusion. A local maximum in the temperatures is evident at $s \approx 10$ due to localized heating via conduction across the substrate. The ratio of this local maximum temperature to the protrusion face temperatures is higher for lower Ra demonstrating the relative importance of substrate conduction at lower Ra.

The effect of Rayleigh number on the dimensionless heat flux across the solid–fluid interface is depicted in Fig. 5. The dimensionless heat flux is defined as

$$\mathbf{Q} = -\frac{R_i}{(Ra\,Pr)^{1/2}}\left(\frac{\mathrm{d}T}{\mathrm{d}N}\right)_i \mathbf{n} \qquad (8)$$

where the subscript i denotes either c or s depending upon whether the interface represents the protrusion–fluid or substrate–fluid interface, respectively. The quantity $(\mathrm{d}T/\mathrm{d}N)_i$ is the dimensionless temperature gradient at the surface and $\mathbf{n}$ the unit outward normal vector. The heat flux in equation (8) is defined to be positive when energy transfer is from the solid to the fluid. The heat flux is calculated via the harmonic mean formulation [16]. As mentioned earlier, the definition of s is given in Table 1.

It must be noted that the heat flux values at the various corners cannot be computed since the outward normal direction is not uniquely determined at those locations. The solid lines joining the computed values at other locations in Fig. 5 are just meant to aid the eye in following the variation of the heat flux over various faces. It is clear from Fig. 5 that the heat flux from the protrusion is not constant on any face, and the variation is a strong function of Ra. The variation over a single protrusion face increases when Ra is lower. On the right side face, for example, the variation in heat flux about the mean is as high as 70% for $Ra = 10^3$. The corresponding level for $Ra = 10^6$ is approximately 25%. Thus it may not be appropriate to model this situation with a constant heat flux condition on the protrusion faces.

For $s < 2$, the heat flux is never negative for $Ra = 10^6$. As Ra decreases, the heat flux closer to the protrusion becomes negative. For $Ra = 10^3$, for example, the transport in the fluid immediately below the protrusion is mainly diffusion-dominated, thus heat is transferred from the fluid to the substrate in that vicinity. We note that for face 5, i.e. the vertical substrate face above the protrusion, the heat flux is negative for $Ra \leqslant 10^5$. Thus the hot fluid is losing energy to the substrate in that region. However, for $Ra = 10^6$, for a small region above the protrusion, the heat flux is positive. This phenomenon occurs because at higher velocities, the main flow largely bypasses the corner in this region, resulting in the substrate losing heat to the fluid in the vicinity of the top face of the protrusion. Note the local maximum in the heat flux at $s \approx 10$ due to the direct conduction effect through the substrate, which is more pronounced at lower Ra. For the value of R_s considered, the substrate is not too efficient in dissipating the energy generated in the protrusion, as is evident from the relative magnitudes of the heat fluxes at the protrusion–fluid and the substrate–fluid interfaces.

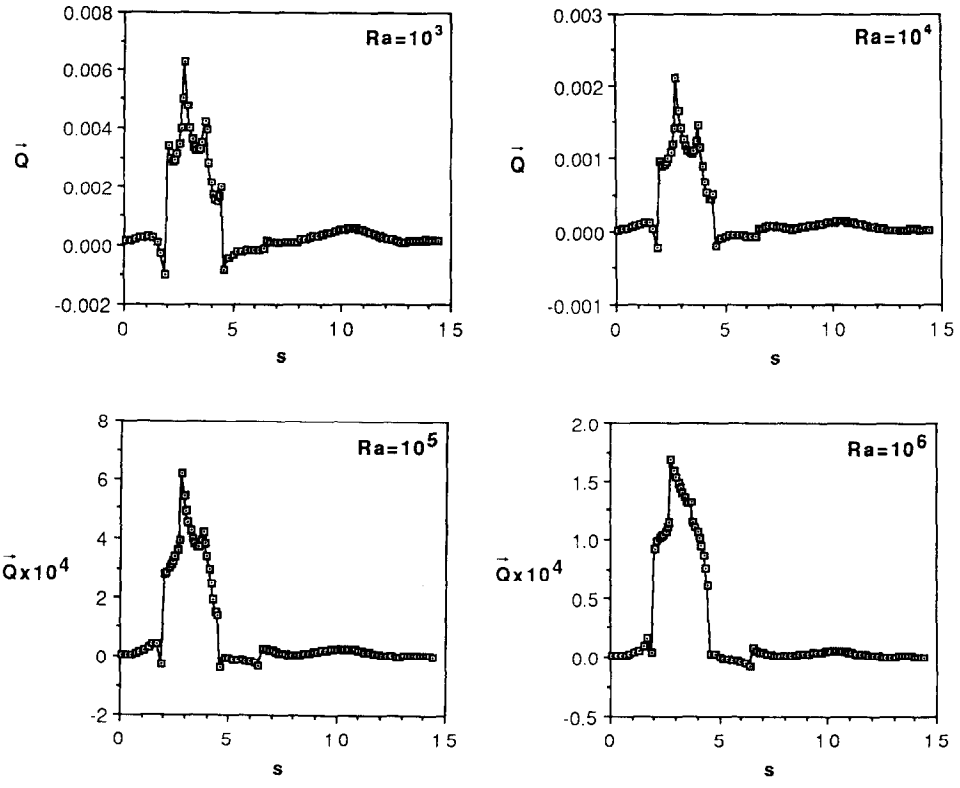

FIG. 5. Effect of Ra on the heat fluxes across the solid–fluid interface when $Pr = 10$, $R_s = 1$ and $R_c = 100$. The distance s is defined in Table 1. The lines joining the symbols are merely to aid the eye.

Figure 6 shows the fractions of the heat generated that pass out through the four protrusion faces. The symbols F_1, F_2, F_3 and F_4 denote the fractions of power that cross the bottom, right (fluid side), top and left (substrate side) faces, respectively. The results are for $R_s = 1$. More than 40% of the generated power is dissipated through the vertical chip face adjacent to the fluid for $Ra \geqslant 10^3$, reaching an asymptote at around 45% for $Ra = 10^5$. Conduction through the substrate accounts for less than 25% of the cooling effect. Thus the results indicate a high potential for cooling enhancement by increasing the substrate conductivity further. The conduction through the substrate becomes less important as Ra increases due to a lower fluid side resistance. For instance, when $Ra \geqslant 10^5$, no more than 10% of the energy is being dissipated via the substrate.

It is interesting to note that the fraction of power dissipated through the bottom of the protrusion remains almost constant at around 25% for the wide range of Ra considered. The fraction dissipated through the top surface is always lower than that through the bottom surface, because of the cooler fluid in contact with the bottom surface and due to the additional fact that the fluid follows the bottom face more closely, and largely bypasses the top face. This results in top faces being slightly hotter than the bottom faces. The vertical face dissipates more heat than the top or bottom faces due to the higher fluid velocities in its vicinity.

Also shown in Fig. 6 is the maximum dimensionless temperature, T_{max}, within the protrusion. As expected, an increase in Ra enhances cooling. The drop in T_{max} with an increase in Ra is more significant at values of Ra below 10^6. At higher Ra other parameters must be adjusted to achieve enhanced cooling. Even though T_{max} values decrease with Ra, actual protrusion temperatures indeed increase with Q for a given set of conditions. As an example, an increase in Ra from 10^3 to 10^5 in Fig. 6 results in a decrease in T_{max} from about 0.2 to 0.1. For uniform fluid properties this implies an increase by a factor of 50 in the actual temperature difference as Q increases by a factor of 100.

5.2. *Effect of* R_s

The streamlines and isotherms for different R_s when $Ra = 10^6$ are seen in Figs. 3(d) and 7. Note that the strength of the secondary cell increases when R_s is higher, due to enhanced substrate conduction. Since the buoyancy effects in the front and the back of the substrate are comparable for $R_s \geqslant 100$, there is no bending of the flow as it leaves the substrate above the protrusion. The bending of the main flow is caused when the velocities on the left-hand side of the sub-

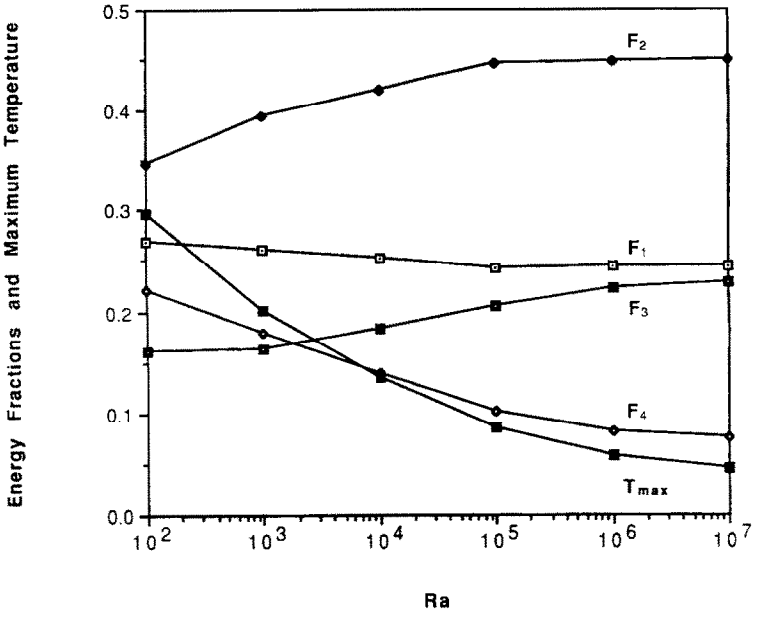

FIG. 6. Energy fractions F_1–F_4 leaving the four protrusion faces and maximum temperature, T_{max}, in the protrusion as a function of Ra. Subscripts 1–4 represent the bottom, fluid-side, top and substrate-side faces of the protrusion, respectively. The computations are for $Pr = 10$, $R_s = 1$ and $R_c = 100$.

strate are low, resulting in a high pressure region there, tending to push the primary cell towards the right. The isotherms clearly reveal that smaller temperature drops result within the substrate as its thermal conductivity increases. The difference between the maximum temperature occurring within the protrusion and the lowest temperature in the substrate is as high as 95% of the overall temperature variation in the enclosure for $R_s \leqslant 1$. The corresponding value is 78% for $R_s = 10$. A superior cooling is achieved with $R_s = 100$, where this value drops to approximately 32%. For such high values of the substrate thermal conductivities, effective heat spreading from the protrusion is achieved, resulting in lower maximum temperatures and lesser thermal stratification in the fluid below the protrusion.

The non-dimensional solid–fluid interface temperatures as a function of s are shown in Fig. 8. The protrusion face temperatures are almost halved when R_s is increased from 1 to 100. Thus higher substrate thermal conductivities are desirable in order to enhance protrusion cooling. On the protrusion surface, the fluid-side vertical face has lower temperatures than the top and bottom faces when $R_s \leqslant 10$. The opposite is true for $R_s = 100$ when the substrate conduction is substantially higher, with the vertical protrusion face adjacent to the fluid being the furthest from the substrate. The substrate temperatures for $R_s = 100$ are almost twice those for $R_s = 1$, indicating a strong influence of substrate conduction. It is seen that the substrate temperatures are fairly uniform, except for $s < 2$, when $R_s = 100$.

Figure 9 shows the dimensionless heat flux across the solid–fluid interface as a function of s. The heat flux patterns do not change substantially on the protrusion–fluid interface for different R_s. The heat flux levels on the protrusion–fluid interface are reduced by more than 60% when R_s is increased from 1 to 100, clearly indicating a heat spreading effect of the high thermal conductivity substrate. The heat flux for $s < 2$ decreases with an increase in s for $R_s = 100$, and increases when $R_s = 1$ and 10. When $R_s = 100$, the substrate is more nearly isothermal compared to when R_s is lower and hence as the fluid travels upward near face 1, it warms up, resulting in a decreasing heat flux from the substrate to the fluid. When $R_s = 1$ and 10, however, the portion of the substrate near $s = 0$ is much cooler than near the protrusion, around $s = 2$. This then results in an increasing heat flux when s increases from 0 to 2. It is interesting to note that an almost constant heat flux results from the back face of the substrate when $R_s = 100$.

The effect of R_s on the fractions of energies F_1–F_4, passing through the bottom, fluid-side, top and substrate-side protrusion faces, respectively, is presented in Fig. 10. These results show that substrate conduction can be neglected only if $R_s \leqslant 0.1$. For such cases almost the entire cooling of the protrusion takes place via conduction within the protrusion and convection into the fluid. However, for $R_s > 0.1$, substrate conduction becomes an important effect, and cannot be neglected. For $R_s = 10^3$, as much as 80% of the heat is dissipated through the substrate. Such an R_s value is typical of a dielectric fluid/ceramic substrate combination. For $R_s > O(10)$, conduction through the substrate is the dominant mode of heat transfer,

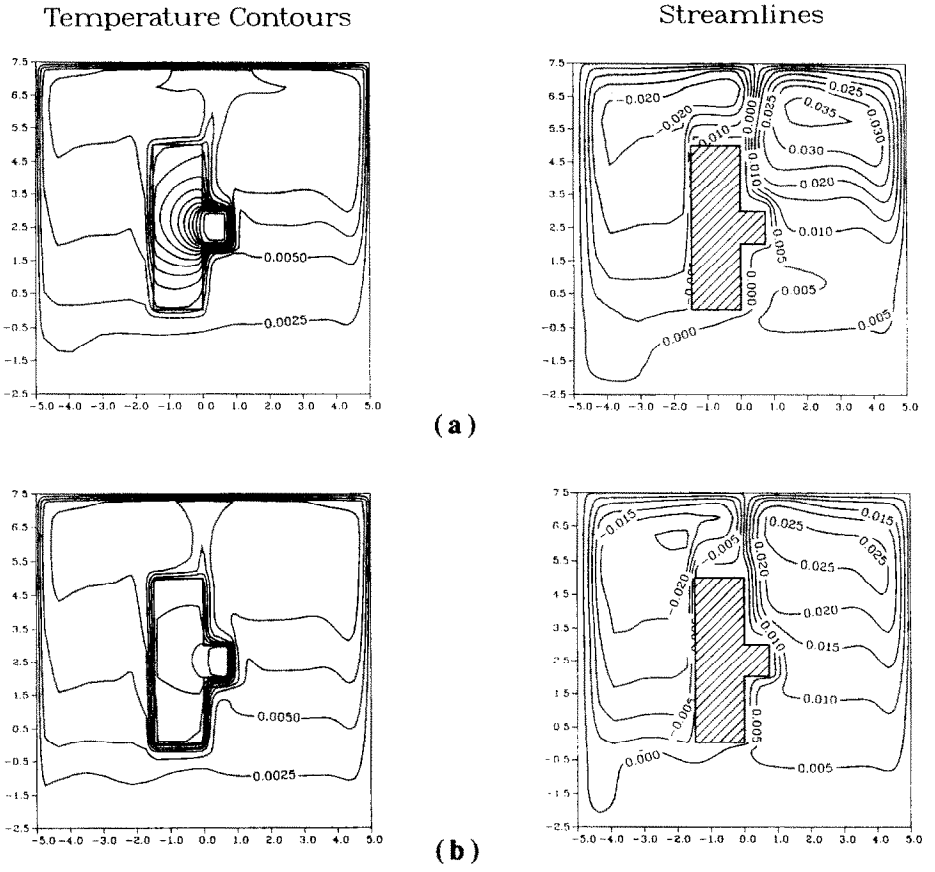

FIG. 7. Streamlines and isotherms for $Ra = 10^6$, $Pr = 10$, $R_c = 100$ when (a) $R_s = 10$ and (b) $R_s = 10^2$.

whereas, it becomes negligible for $R_s < O(0.01)$. For many practical situations since R_s is larger than 0.1 the effects of substrate conduction must be accounted for. It is interesting to note that the fractional levels as well as the trends are similar for $Ra = 10^5$ and 10^6.

The conduction through the substrate also has a pronounced effect on the maximum temperatures occurring inside the protrusion. Figure 11 shows the effect of Ra and R_s on the maximum protrusion temperature, T_{max}. The trends show that T_{max} decreases with an increase in R_s for all Ra. The maximum temperature seems to be reaching an asymptote for $R_s < 1$ or $R_s > 100$. These trends could be easily explained with the results shown in the earlier figure. When $R_s = 1$, the conduction through the substrate is a minor fraction of the generated energy. Thus it is expected that T_{max} will not increase substantially when R_s decreases further. The opposite effect occurs when $R_s = 100$. The conduction through the substrate for this value of R_s is large enough so that a further increase in R_s is expected to bring down the temperature levels in the protrusion only marginally. In the intermediate range, namely $1 \leqslant R_s \leqslant 100$, T_{max} changes substantially because the fraction of energy passing into the substrate shows a wide variation. It is interesting to note that in this range, T_{max} varies almost linearly with log (R_s). From a practical point of view, R_s should be at least 100 to achieve a good cooling effect.

6. COMPARISONS WITH EXISTING MEASUREMENTS

Comparisons of the present numerical simulations were made with the experimental data of ref. [19]. The experiments examined the natural convection cooling of a column of stainless-steel protrusions mounted on a vertical Plexiglas surface in water. The protruding elements were 23.9 mm long, 7.8 mm high and extended 6.1 mm from the Plexiglas substrate, so that $w/h = 0.782$ for numerical calculations. These geometric dimensions were chosen to simulate 20 pin Dual In-line Packages (DIPS). Heating was achieved by placing 0.18 mm thick foil heaters at the bases of the elements.

The experiments revealed that the bottom element in the column was unaffected by downstream components due to the boundary layer like transport. This was confirmed by powering only the lowest com-

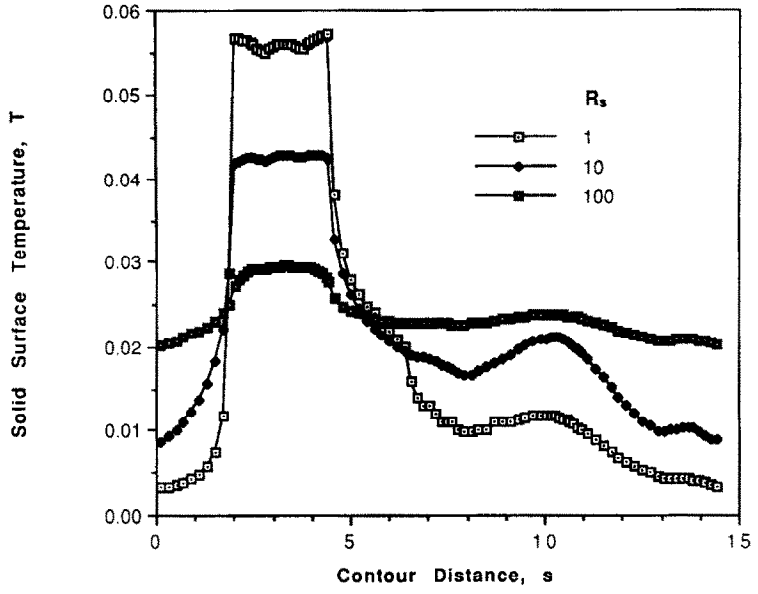

FIG. 8. Comparison of the temperatures on the solid–fluid interface for different R_s when $Ra = 10^6$, $Pr = 10$ and $R_c = 100$. The definition of s is given in Table 1.

ponent and comparing the resulting face temperatures with those measured with the entire column powered. Also, the flow in the plane through the component centers was largely two-dimensional for the power levels examined. Thus the present two-dimensional computational model appeared to be a suitable simulation of the transport in the central plane of the lowest component in the experimental configuration.

The experimental runs performed in ref. [19] did not indicate any oscillatory flow patterns at long times. Both in the present numerical computations and in ref. [19] Ra was below 10^7. Flow oscillations were reported for a single protrusion in a smaller enclosure for a significantly larger $Ra = 1.55 \times 10^8$ [10]. It is interesting to observe that despite oscillations in the flow patterns at these higher Ra levels, the heat flux from the protrusion varied by less than 2% [10].

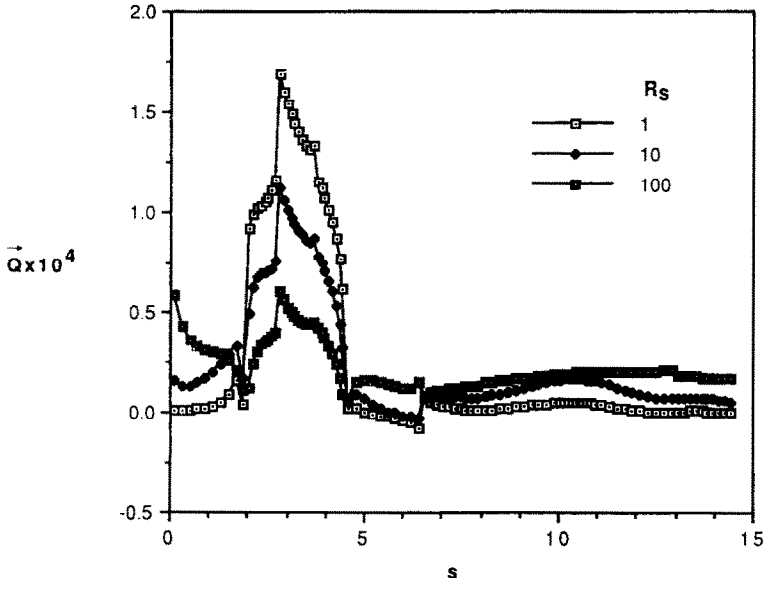

FIG. 9. The effect of R_s on the heat flux leaving the solid surface for $Ra = 10^6$, $Pr = 10$ and $R_c = 100$. The contour distance s is defined in Table 1. The lines joining the symbols are merely to aid the eye.

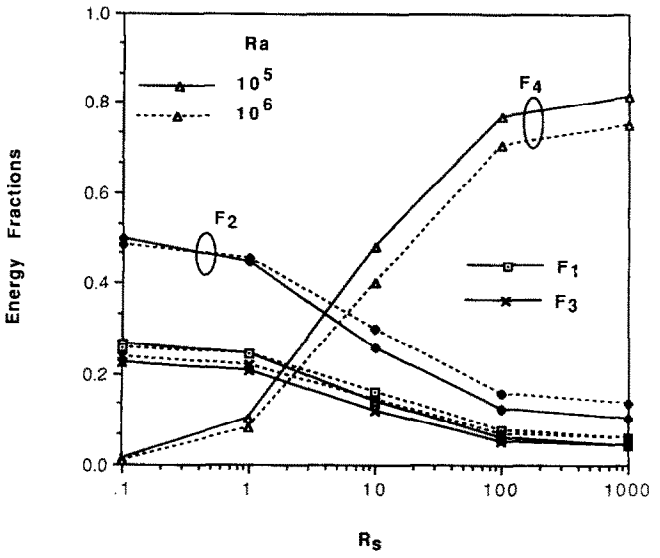

FIG. 10. Energy fractions F_1–F_4 for different Ra and R_s when $Pr = 10$ and $R_c = 100$. Subscripts 1–4 denote the bottom, right, top and left surface of the protrusion, respectively.

6.1. *Effect of free surface boundary conditions and enclosure size*

Since the tank used in the experiments had a free surface on the top instead of a solid wall in the numerical model, the effect of the free surface condition was determined. It was found that the temperatures within and in the vicinity of the protrusion differed by a negligible amount when either a free-surface or a solid-wall boundary condition was used at the top surface of the enclosure when $H/h = 11$. Increasing the enclosure size and the substrate length further (as was the case in the experiments) also had an insignificant effect on the computed protrusion surface temperatures. Increasing the enclosure size required a larger number of grid points and hence greater computational time. Thus the numerical results reported in the following were obtained with $H/h = 11$.

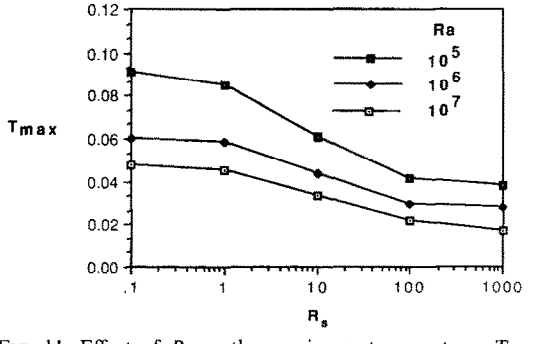

FIG. 11. Effect of R_s on the maximum temperature, T_{max}, occurring within the protrusion for different Ra.

6.2. *Effect of heater size*

In a few typical runs it was found that a negligible difference in the protrusion-face temperatures resulted if equivalent heating took place in a narrow region at the base of the protrusion rather than with uniform heat generation over the entire protrusion. This result could be attributed to the high thermal conductivity of the protrusion, so that it acted as an effective heat spreader. Also, the computational times were almost tripled, when the equivalent heating was confined to a very narrow region. Thus the numerical simulations were made with uniform volumetric heat generation in the entire protrusion.

6.3. *Protrusion face temperatures*

The comparisons with experimental data are for the situation when only the lowest block was powered in a vertical column. The protrusion surface temperatures were measured at three locations in a vertical plane through the geometric center of the element. These positions correspond to the centers of faces 2, 3 and 4 in Fig. 1. The properties of water were evaluated from ref. [20] at a mean film temperature, chosen as the average of the measured levels at various component face centers and the ambient.

A comparison between the experimental and the numerical protrusion-face temperatures is shown in Fig. 12. The numerical predictions are for $R_c = 24.2$, $R_s = 0.24$, $S_b/h = 2.5$, $d/h = 2.5$, $L_t/h = 2.5$, $S_t/h = 2.5$, $d_t/h = 1.625$ and $w/h = 0.78$. Note that $Pr \cong 8$ for all the data points. An $Ra = 0.6 \times 10^5$ corresponds to an actual heating rate of 0.2 W in the stainless-steel blocks. As expected, both the numerically computed and measured temperatures show a decrease when the Rayleigh number increases. The

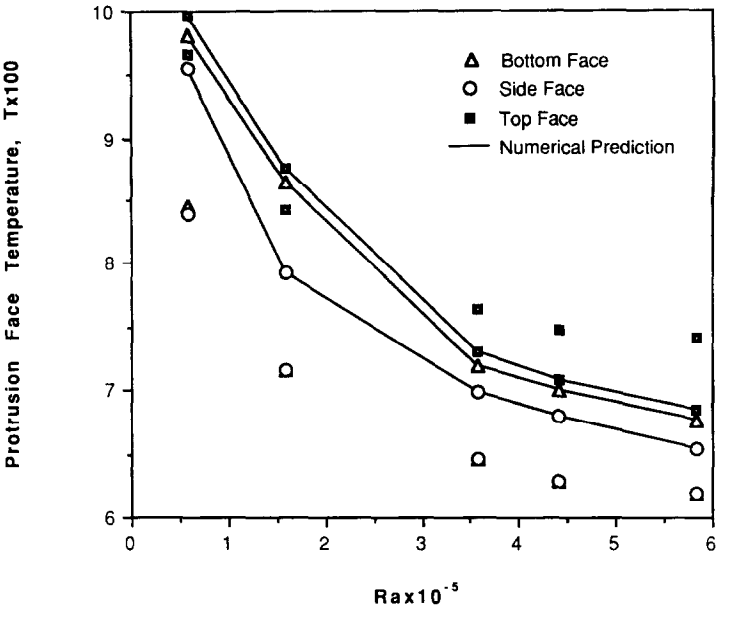

FIG. 12. A comparison of the numerically predicted (solid lines) and experimentally measured (isolated symbols) protrusion face temperatures.

top face of the protrusion is the warmest, and the side face is the coolest, as found both in the experiments and the numerical predictions. This is due to the fact that the flow follows the protrusion closely adjacent to the side surface, and largely bypasses the top surface. Since the three-dimensional nature of the flow in the experiments is more pronounced near the bottom face, discrepancies between the experimental and numerical predictions are the largest, in general, at that face. The measured temperatures are somewhat lower than the predicted values, for the side and the bottom faces, which could be attributed to the three-dimensional effects.

The discrepancies in the predicted and measured temperatures range from 3 to 17%. These deviations are the net result of the experimental uncertainties and the three-dimensional nature of the transport in the experimental situation. Based on these comparisons it is clear that the two-dimensional formulation may be used as a reliable tool to predict the performance of certain electronic components, such as DIPs, without incurring prohibitively high costs associated with three-dimensional computations. It is expected, however, that in situations where the transport is strongly three-dimensional, the present formulation may not be appropriate.

7. CONCLUSIONS

A numerical study was performed to investigate the heat transfer and fluid flow arising from a substrate-mounted protruding heat source immersed in a liquid-filled two-dimensional enclosure. The model accounted for conduction heat transfer within the protrusion and substrate and the coupled natural convection in the fluid. Numerical predictions agreed favorably with the wall plume similarity solution for the limiting case of a vanishingly small protrusion mounted on an adiabatic substrate.

A parametric study was conducted for a range of Ra, Pr and R_s that may be encountered in electronic cooling applications. The flow in the enclosure below the protrusion was thermally stratified. A marked change in the flow pattern was visible when Ra was increased beyond 10^5 with the secondary cell moving from the back of the substrate to the top of the substrate. Higher Ra enhanced protrusion cooling and diminished the importance of substrate conduction. A variation in Pr from 10 to 10^3 did not affect the solid temperatures substantially. A high value of R_s enhanced the cooling of the protrusion due to an increase in the secondary circulation at the back of the substrate. Substrate conduction was the dominant cooling effect for $R_s > 10$. As much as 80% of the power generated by the protrusion was dissipated by the substrate when $R_s = 10^3$. The results indicated that for most actual situations, the substrate conduction effects cannot be neglected. Also, in many applications it may be inappropriate to prescribe simple boundary conditions such as constant temperature or heat flux on the protrusion faces and solve for the governing equations only in the fluid.

Computed protrusion surface temperatures compared favorably with experimental results for a similar configuration. This indicates that two-dimensional models may provide reasonable predictions of com-

ponent surface temperatures in some electronic packages.

Acknowledgement—The authors are grateful for the support of this work by a grant from the U.S. Naval Weapons Support Center, Crane, Indiana.

REFERENCES

1. R. C. Chu, Heat transfer in electronic systems, *Proc. Eighth Int. Heat Transfer Conf.*, San Francisco, p. 293 (1986).
2. W. Nakayama, Thermal management of electronic equipment: a review of technology and research topics. In *Advances in Thermal Modeling of Electronic Components and Systems* (Edited by A. Bar-Cohen and A. D. Kraus), Vol. 1, p. 1. Hemisphere, Washington, DC (1988).
3. F. P. Incropera, Convection heat transfer in electronic equipment cooling, *ASME J. Heat Transfer* **110,** 1097 (1988).
4. Y. Jaluria, Interaction of natural convection wakes arising from thermal sources on a vertical surface, *ASME J. Heat Transfer* **107,** 883 (1985).
5. S. Lee and M. M. Yovanovich, Conjugate heat transfer from a vertical plate with discrete heat sources under natural convection, ASME Paper No. 89-WA/EEP-9 (1989).
6. M. Afrid and A. Zebib, Natural convection air cooling of heated components mounted on a vertical wall, *Numer. Heat Transfer* **A15,** 243 (1989).
7. E. Baker, Liquid cooling of microelectronic devices by free and forced convection, *Microelectron. Reliability* **11,** 213 (1972).
8. E. Baker, Liquid immersion cooling of small electronic devices, *Microelectron. Reliability* **12,** 163 (1973).
9. K. A. Park and A. E. Bergles, Natural convection heat transfer characteristics of simulated microelectronic chips, *ASME J. Heat Transfer* **109,** 90 (1987).
10. M. D. Kelleher, R. H. Knock and K. T. Yang, Laminar natural convection in a rectangular enclosure due to a heated protrusion on a vertical wall—Part I: experimental investigation, *Proc. Second ASME/JSME Therm. Engng Joint Conf.*, Honolulu, p. 169 (1987).
11. M. Keyhani, V. Prasad and R. Cox, An experimental study of natural convection in a vertical cavity with discrete heat sources, ASME Paper No. 87-HT-76 (1987).
12. L. Chen, M. Keyhani and D. R. Pitts, An experimental study of natural convection heat transfer in a rectangular enclosure with protruding heaters, presented at the Natn. Heat Transfer Conf., Houston, Texas (1988).
13. Y. Joshi, M. D. Kelleher and T. J. Benedict, Natural convection immersion cooling of an array of simulated electronic components in an enclosure filled with dielectric fluid. In *Heat Transfer in Electronic and Microelectronic Equipment* (Edited by A. E. Bergles), p. 445. Hemisphere, Washington, DC (1990).
14. J. J. Lee, K. V. Liu, K. T. Yang and M. D. Kelleher, Laminar natural convection in a rectangular enclosure due to a heated protrusion on one vertical wall—Part II: numerical simulation, *Proc. Second ASME/JSME Therm. Engng Joint Conf.*, Honolulu, p. 179 (1987).
15. K. V. Liu, K. T. Yang and M. D. Kelleher, Three dimensional natural convection cooling of an array of heated protrusions in an enclosure filled with a dielectric fluid, *Proc. Int. Symp. on Cooling Technology for Electronic Equipment*, Honolulu, p. 179 (1987).
16. S. V. Patankar, *Numerical Heat Transfer and Fluid Flow*. Hemisphere/McGraw-Hill, New York (1980).
17. Y. Jaluria and B. Gebhart, Buoyancy-induced flow arising from a line thermal source on an adiabatic vertical surface, *Int. J. Heat Mass Transfer* **20,** 153 (1977).
18. Product Manual, Fluorinert Electronic Liquids, 3M Corporation, St. Paul, Minnesota (1985).
19. Y. Joshi, T. Willson and S. J. Hazard, An experimental study of natural convection from an array of heated protrusions on a vertical surface in water, *ASME J. Electron. Packaging* **111,** 121 (1989).
20. F. P. Incropera and D. P. Dewitt, *Introduction to Heat Transfer*. Wiley, New York (1985).

CONVECTION NATURELLE AUTOUR D'UNE PROTUBERANCE MONTEE SUR SUBSTRAT ET GENERATRICE DE CHALEUR DANS UNE CAVITE BIDIMENSIONNELLE EMPLIE DE LIQUIDE

Résumé—On étudie l'écoulement et le transfert thermique de convection naturelle autour d'une source de chaleur protubérante montée sur substrat et immergée dans un liquide à l'intérieur d'une cavité. Le modèle considère le transfert thermique dans la protubérance et le substrat ainsi que la convection naturelle couplée dans le fluide. Des prédictions numériques sont obtenues pour un large domaine de nombres de Rayleigh et de Prandtl et de rapports des conductivités thermiques du substrat et du fluide qui peuvent être rencontrés dans le refroidissement par immersion des composants électroniques. Beaucoup de situations réelles prescrites par des conditions thermiques simplistes à la surface solide sont trouvées inappropriées. L'accroissement du nombre de Rayleigh au delà de 10^6 et de la conductivité thermique du substrat au delà de 100 fois celle du liquide produit seulement une décroissance marginale des températures maximales. Les températures calculées de la surface de la protubérance se comparent favorablement aux valeurs expérimentales pour une configuration semblable.

NATÜRLICHE KONVEKTION AN EINEM WÄRMEERZEUGENDEN VORSPRUNG IN EINEM FLÜSSIGKEITSGEFÜLLTEN ZWEIDIMENSIONALEN HOHLRAUM

Zusammenfassung—Strömung und Wärmeübergang bei natürlicher Konvektion an einem wärmeerzeugenden Vorsprung in einem flüssigkeitsgefüllten quadratischen Hohlraum werden untersucht. Das Modell berücksichtigt den Wärmetransport innerhalb des Vorsprungs und des darunterliegenden Substrats sowie bei der gekoppelten natürlichen Konvektion im Fluid. Für einen weiten Bereich von Rayleigh- und Prandtl-Zahlen sowie von Verhältnissen der Wärmeleitfähigkeit des Substrats zu derjenigen der Flüssigkeit—wie sie zum Beispiel bei Flüssigkeitskühlung elektronischer Bauelemente vorkommen—werden numerische Berechnungen ausgeführt. Für viele praktisch interessierende Situationen ist die Annahme der üblichen einfachen Randbedingungen für den Wärmeübergang an festen Oberflächen ungenügend. Eine Vergrößerung der Rayleigh-Zahl über 10^6 und der Wärmeleitfähigkeit des Substrats über das Hundertfache der Flüssigkeit führt nur zu einer geringfügigen Verringerung der maximalen Temperaturen. Die berechneten Temperaturen des Vorsprungs stimmen recht gut mit verfügbaren Versuchsergebnissen für ähnliche Konfigurationen überein.

ЕСТЕСТВЕННАЯ КОНВЕКЦИЯ ОТ ВЫСТУПАЮЩЕГО ИСТОЧНИКА ТЕПЛА, УСТАНОВЛЕННОГО НА ПОДЛОЖКЕ В ЗАПОЛНЕННОЙ ЖИДКОСТЬЮ ДВУМЕРНОЙ ПОЛОСТИ

Аннотация—Исследуются естественноконвективное течение и теплоперенос от установленного на подложке выступающего источника тепла, погруженного в заполненную жидкостью квадратную полость. Модель описывает теплоперенос в выступе и подложке, а также взаимосвязанную естественную конвекцию в жидкости. Получены численные результаты для широкого диапазона чисел Рэлея и Прандтля, а также значений отношения коэффициентов теплопроводности подложки и жидкости, которые могут встречаться при охлаждении электронных узлов посредством погружения в жидкость. Увеличение числа Рэлея свыше 10^6 и коэффициента теплопроводности подложки более, чем в 100 раз по сравнению с жидкостью приводит лишь к незначительному снижению максимальных температур. Расчетные значения температуры поверхности выступа удовлетворительно согласуются с имеющимися экспериментальными разультатами для аналогичной конфигурации.